Electronic Supplementary Material (ESI) for Environmental Science: Nano.

Supporting File

Utilization of Lead based saturated adsorbent for the fabrication of battery like hybrid asymmetric supercapacitor

Sourav Acharya[a], Shrabani De[a], Ayon Ganguly[a], Brijesh K. Mishra*[,b], and Ganesh Chandra Nayak,*[,a]

[a]Department of Chemistry and Chemical Biology, Indian Institute of Technology (ISM), Dhanbad-826004 Jharkhand, India

[b]Department of Environmental Science and Engineering, Indian Institute of Technology (ISM), Dhanbad-826004 Jharkhand, India

* E-mail Id of Corresponding authors: gcnayak@iitism.ac.in, brijesh@iitism.ac.in

S1. Synthesis of MnO_2

MnO_2 was synthesized using a simple thermal treatment method [1]. In a typical process, $MnCO_3$ (Mn content 42-46 %, SRL India Pvt. Ltd.) was heated in a ceramic crucible at 300 °C for 12 hours in a muffle furnace in air to obtain pristine MnO_2. This was used as the positive electrode in supercapacitor fabrication.

S2. Characterization of the samples

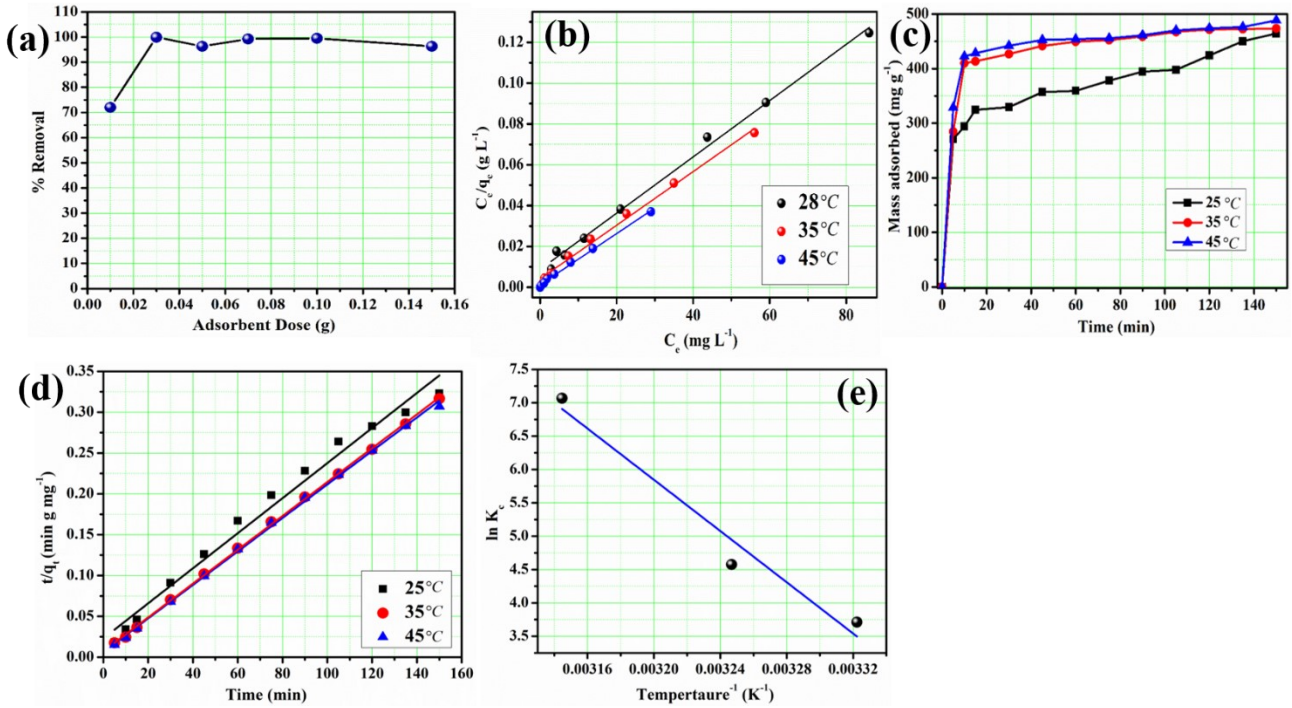

Figure S1: (a) Dose optimization, (b) Isotherm study, (c) Adsorption time with variation

in temperature, (d) Fit of adsorption data to second-order kinetics model, and (e) Thermodynamic parameters calculation of the Pb adsorption

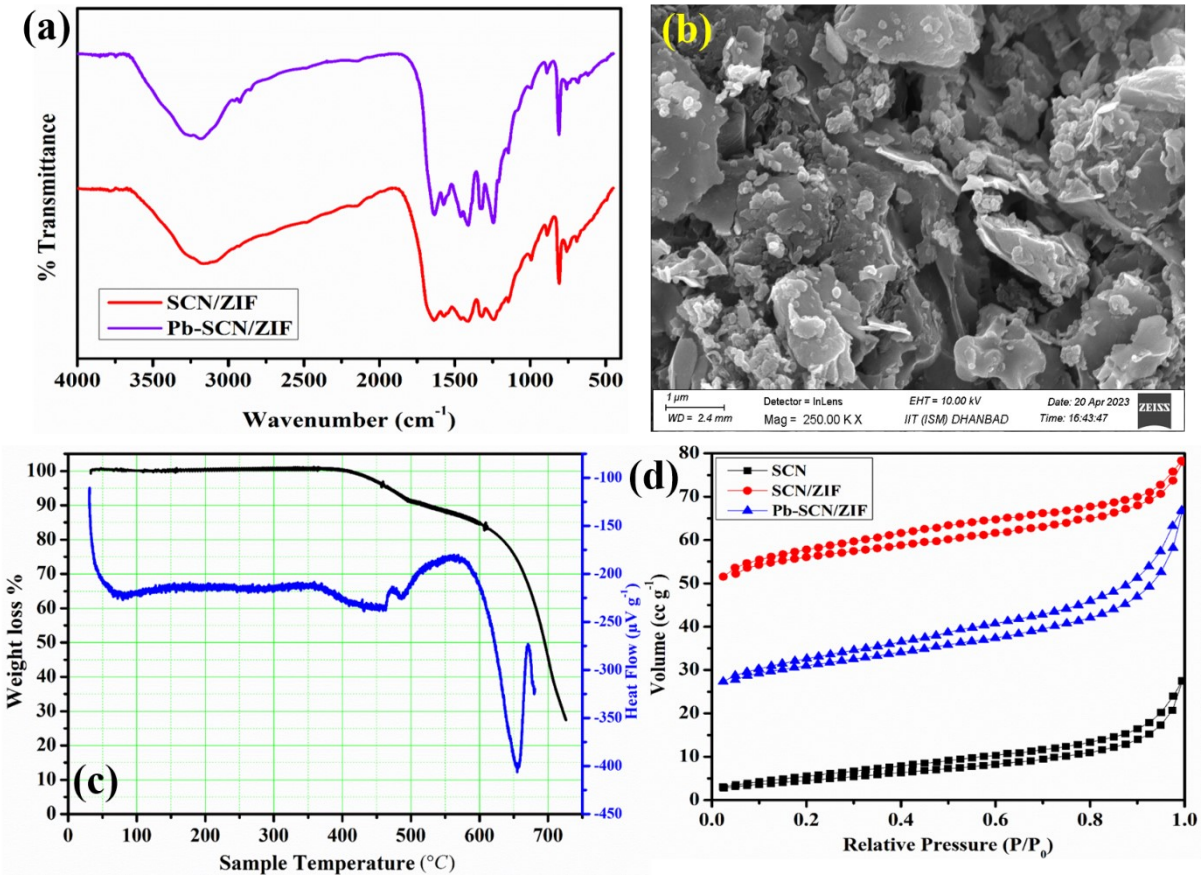

Figure S2: (a) FTIR plot of adsorbent before and after adsorption, (b) FESEM image of Pb-SCN/ZIF, (c) TGA of SCN/ZIF composite, and (d) BET analysis of the samples.

Table S1: BET data of the composites.

Sample	Surface Area ($m^2 g^{-1}$)	Total Pore volume ($cc\ g^{-1}$)	Avg. Pore radius (nm)
SCN	16.89	0.576	4.9
SCN/ZIF	176.6	0.444	1.395
Pb-SCN/ZIF	100.05	0.379	2.095

Table S2: RAMAN data of the composites.

Sample	D band (cm^{-1})	G band (cm^{-1})	I_D/I_G ratio
Carbon@ZIF	1336	1582	1.04
H@SCN/ZIF	1323	1585	1.03
H@Pb-SCN/ZIF	1322	1580	1.07

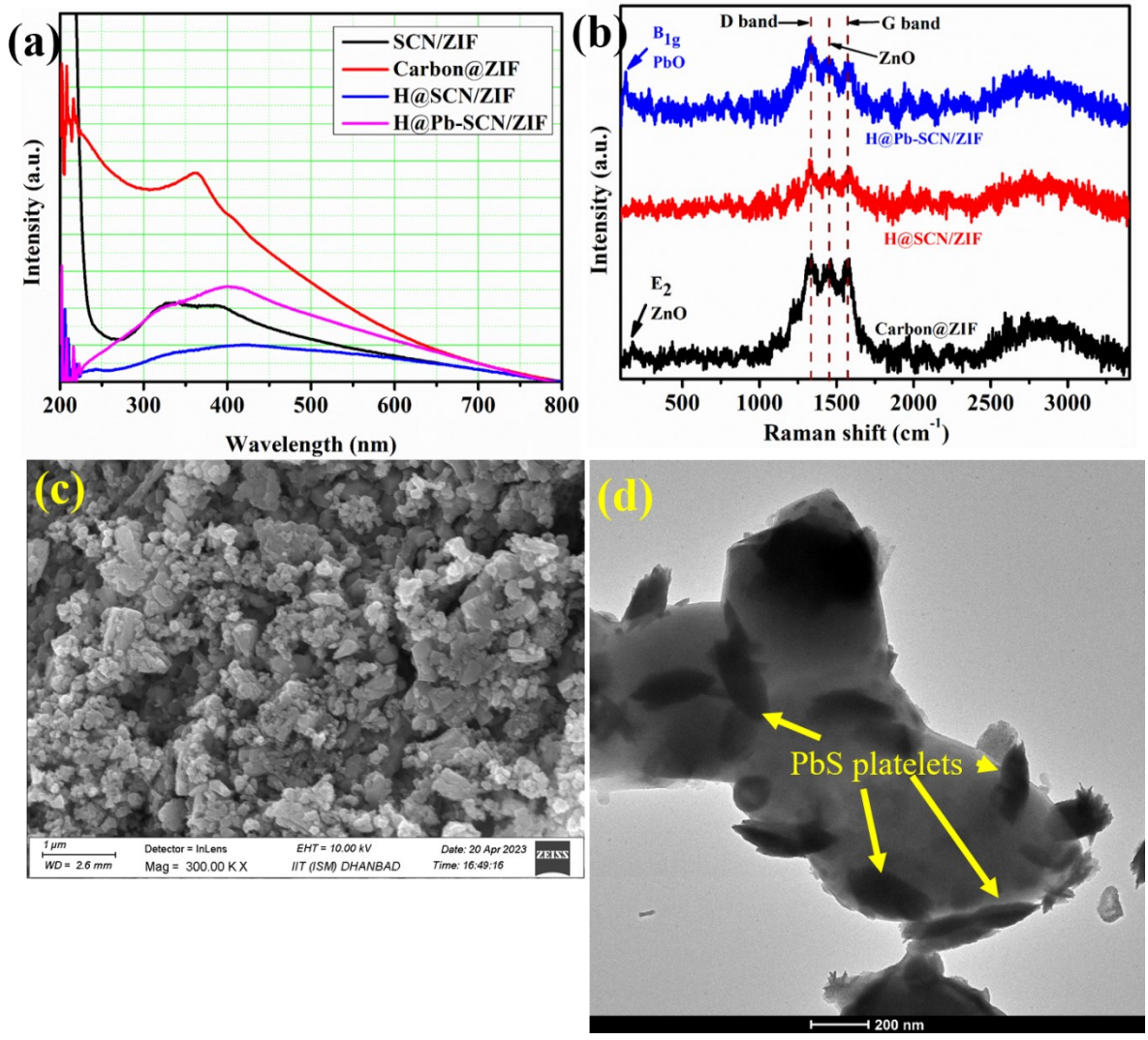

Figure S3: (a) UV-Vis analysis of after heat treatment composites, (b) RAMAN analysis of after heat treatment composites, (c) FESEM image of Carbon@ZIF, and (d) HRTEM image of H@Pb-SCN/ZIF.

S3. Electrochemical study

S3.1. Trasatti method analysis:

The following steps are obeyed for this theoretical analysis. The corresponding areal capacitance of H@Pb-SCN/ZIF was calculated using the following equation:

$$C = \frac{S}{2.\Delta V.\upsilon}$$ (Equation S1)

Where, C is the areal capacitance in F cm^{-2}, ΔV is the voltage window in V, υ is the scan rate in V s^{-1} and S is the area enclosed by the corresponding cyclic voltammograms in A V cm^{-2}. Reciprocal of the calculated areal capacitances (C^{-1}) and the square root of the scan rates ($\upsilon^{-1/2}$) should be in linear co-relationship assuming ion diffusion follows a semi-infinite diffusion pattern [2].

$C^{-1} = \text{Constant}.\ \upsilon^{1/2} + C_T^{-1}$ (Equation S2)

Where is C_T the total capacitance, which can be considered as the sum of electron double-layer capacitance and pseudocapacitance and can be calculated from intercept of the Y-axis of C^{-1} and $\upsilon^{1/2}$ plot [3]. Again, calculated areal capacitances show linear relationship with the reciprocal of the square root of the scan rates assuming a semi-infinite diffusion pattern [4].

$C = \text{Constant}.\ \upsilon^{-1/2} + C_{EDL}$ (Equation S3)

Here, $C_{EDL}$is the maximum electron double layer capacitance and it can be calculated from intercept in Y-axis of plot of C and $\upsilon^{-1/2}$ [3]. Subtracting the electron double layer capacitance (C_{EDL}) from total capacitance (C_T) gives the maximum pseudocapacitance (C_{PS}). So the capacitance contribution can be calculated by using the following equation:

$$C_{EDL}\ \% = \frac{C_{EDL}}{C_T} \times 100$$ (Equation S4)

$$C_{PS}\ \% = \frac{C_{PS}}{C_T} \times 100$$ (Equation S5)

Table S3: C_{sp} of H@Pb-SCN/ZIF at different scan rates in 0 to -0.65 V voltage window in 3-elctrode.

Current density (A g^{-1})	C_{sp} (F g^{-1})
2	2052
3	970
4	800
5	707
10	570

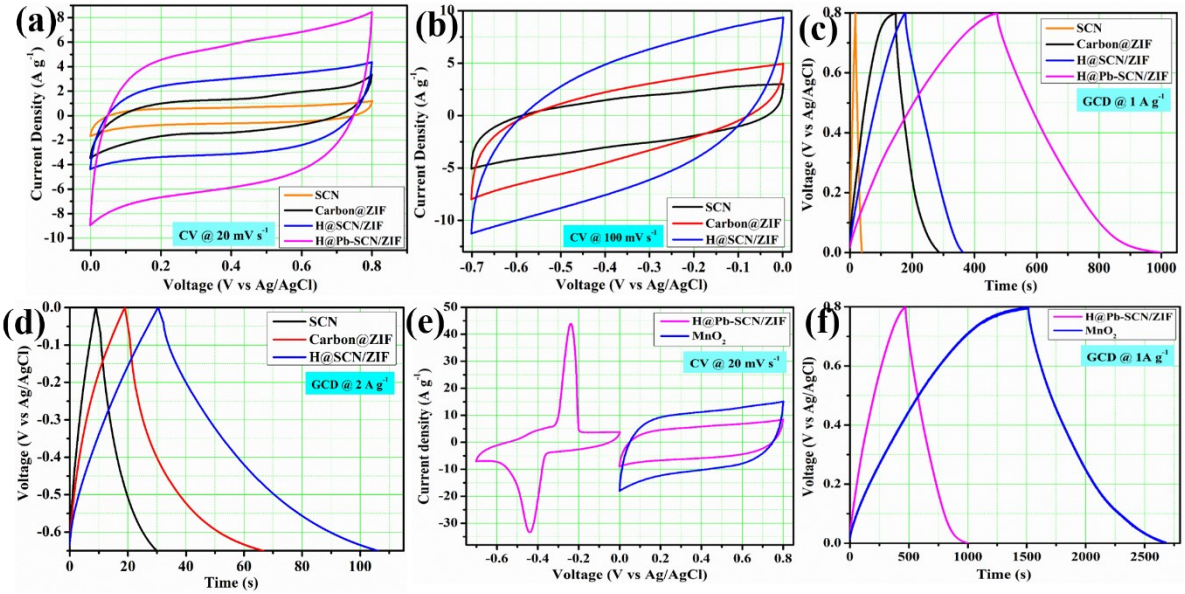

Figure S4: (a) CV comparison of the samples in 0 to 0.8 V, (b) CV comparison of the samples in 0 to -0.7 V, (c) GCD comparison of the samples in 0 to 0.8 V, (d) GCD comparison of the samples in 0 to -0.7 V, (e) CV of MnO_2 compared to H@Pb-SCN/ZIF, and (f) GCD of MnO_2 compared to H@Pb-SCN/ZIF

$$\frac{m_+}{m_-} = \frac{C_{sp-} \times \Delta V_-}{C_{sp+} \times \Delta V_-} \qquad \textbf{(S1)}$$

Where, C_{sp+} and C_{sp-} are the specific capacitance of the devices in Wh kg^{-1} for the material used in cathode and anode, respectively calculated in 3-electrode study, while ΔV_+ and ΔV_- are the voltage window of the material used in cathode and anode, respectively in 3-electrode study.

Table S4: C_{sp}, ED and PD of supercapacitor at different voltage window.

Potential Window (V)	C_{sp} ($F\ g^{-1}$)	ED ($Wh\ kg^{-1}$)	PD ($W\ kg^{-1}$)
0.8	27	2.4	800
1	47	6.6	1000
1.2	121	24.3	1200
1.4	193	52.7	1400
1.5	225	70.4	1500

Table S5: C_{sp}, ED and PD of supercapacitor at different current density.

Current density ($A\ g^{-1}$)	C_{sp} ($F\ g^{-1}$)	ED ($Wh\ kg^{-1}$)	PD ($W\ kg^{-1}$)
0.5	364	113.7	750
1	225	70.4	1500
2	134	41.9	3000
3	68	21.3	4500
4	43	13.3	6000

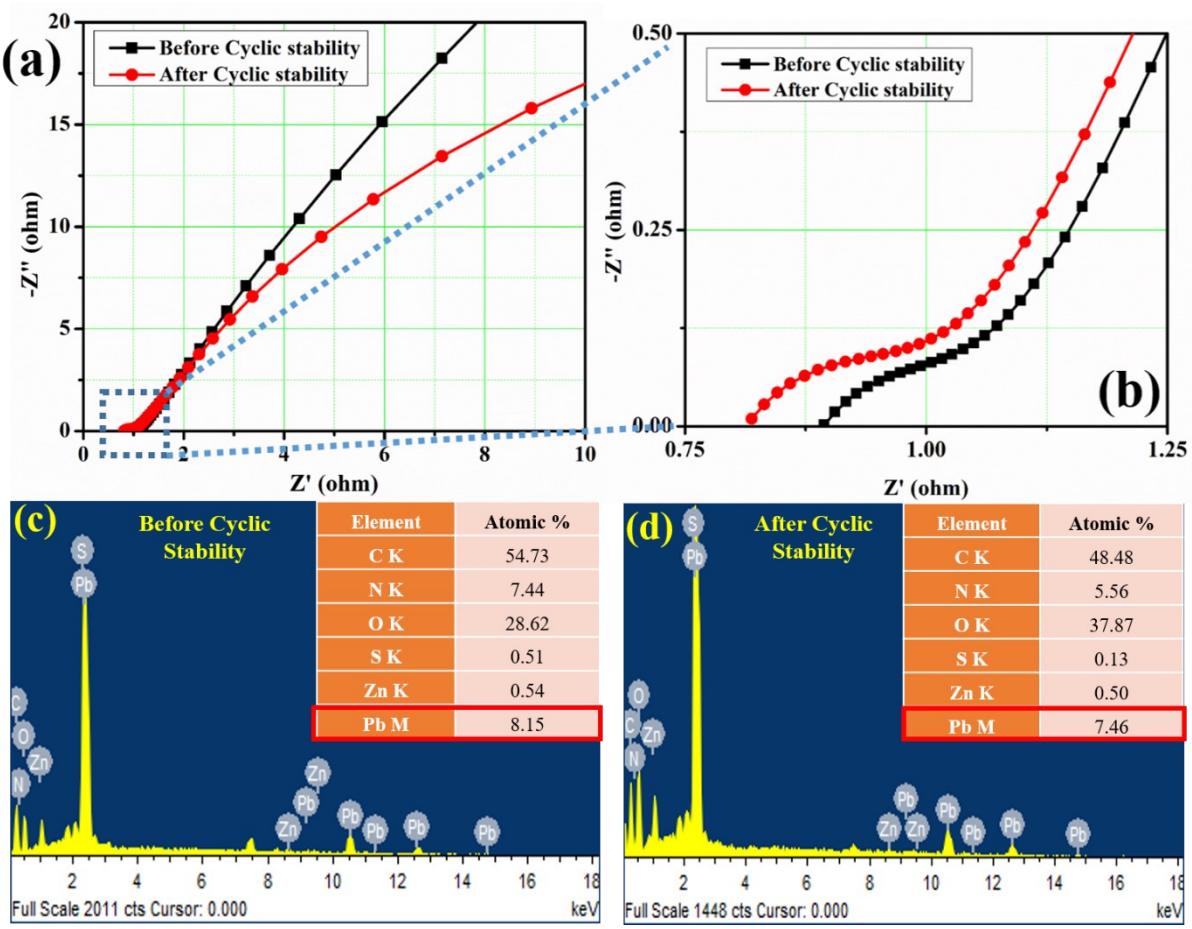

Figure S5: (a) and (b) EIS analysis of the supercapacitor before and after cyclic stability, and FESEM-EDX analysis of the electrodes (c) Before cyclic stability, and (d) After cyclic stability analysis.

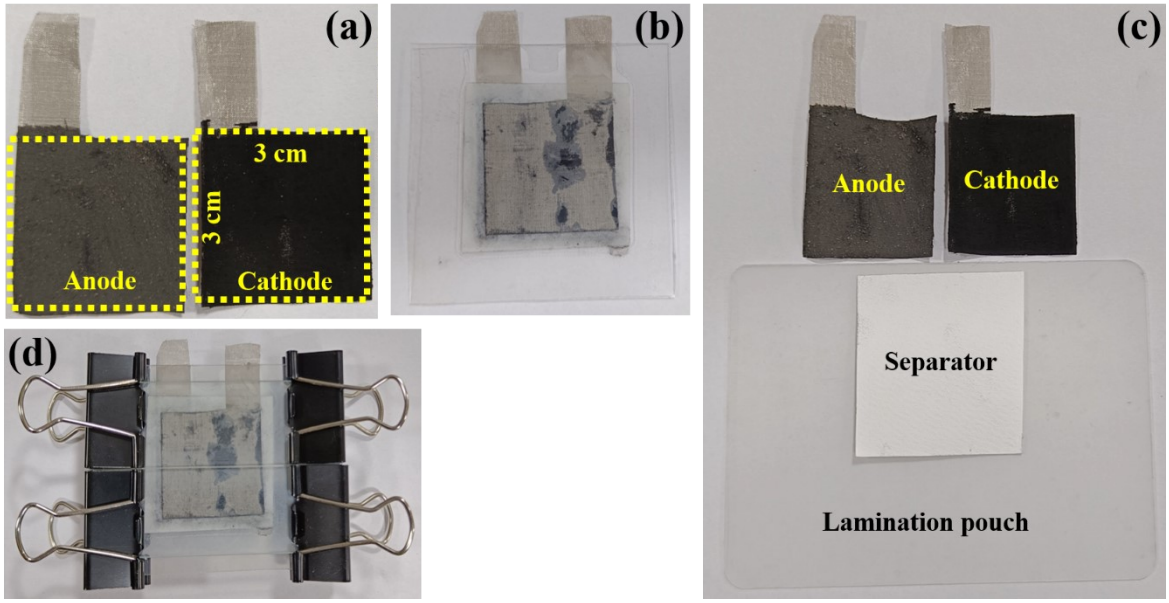

Figure S6: (a) Coated electrodes, (b) Fabricated device, (c) Components of the supercapacitor, and (d) Device as used for electrochemical testing.

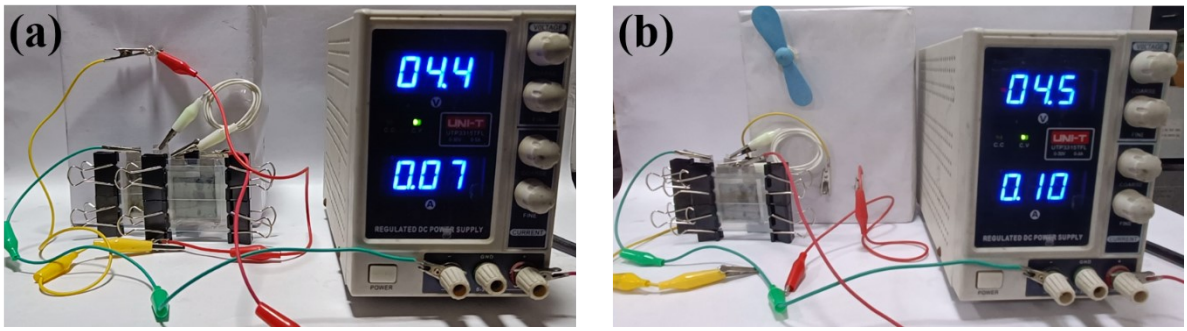

Figure S7: (a) Charging setup for glowing green LED, and (b) Charging setup for operating 2 V DC fan.

Table S6: Comparison of the fabricated supercapacitor with recently reported devices.

Sample	Electro lyte	Voltage window (V)	Current density (A g^{-1})	C_{sp} (F g^{-1})	ED (Wh kg^{-1})	PD (W kg^{-1})	Cyclic stability	Ref.
MnO_2-$FeSe_2$ //AC	KOH	1.7	1	148	55.39	850	95 % after 10000 cycles	[5]
3D-C-$NiCo_2O_4$/Ni// 3D-Fe_3S_4@NiCo /SS	2 M KOH	1.6	1	150	49.8	782	70 % after 10000 cycles	[6]
Cu-MOF//AC	1 M KOH	1.8	0.6	173.4	41	2400	92 % after 1000 cycles	[7]
$Cu_{0.27}Co_{2.73}O_4$ //AC	1 M KOH	1.6	0.5	100.6	35.78	400	86.9 % after 20000 cycles at 5 A g^{-1}	[8]
FeP_2/Co_2P/Ni //AC	6 M KOH	1.6	0.5	46 mAh g^{-1}	41.2	445	91 % after 10000 cycles at 5 A g^{-1}	[9]
MnO_{2-x} @CoS// Porous Carbon	3 M KOH	1.7	0.7	147 C g^{-1}	34.72	597.24	89.6 % after 9000 cycles at 4 A g^{-1}	[10]
Fe_2O_3@α-$Ni(OH)_2$//AC	1 M KOH	1.4	1	63.3 C g^{-1}	44.51	2465	90.5 % after 4000 cycles at 10 A g^{-1}	[11]
TiN/C//TiC/C	1 M Na_2SO_4	1.8	0.5	103	45.2	535.2	83 % after 4000 cycles	[12]
MnO_2//Pb saturated sample	**1 M Na_2SO_4**	**1.5**	**0.5**	**364**	**113.7**	**750**	**108 % after 10000 cycles at 10 A g^{-1}**	**This Work**

NB: Device denoted as Positive electrode//Negative Electrode.

Reference:

[1] Y. Liu, P. Zhang, J. Zhan, and L. Liu, Heat treatment of $MnCO_3$: An easy way to obtain efficient and stable MnO2 for humid O3 decomposition, 463 (2019) 374-385.

[2] S. Ardizzone, G. Fregonara, and S. Trasatti, "Inner" and "outer" active surface of RuO_2 electrodes, 35(1) (1990) 263-267.

[3] Y.H. Lee, K.H. Chang, and C.C. Hu, Differentiate the pseudocapacitance and double-layer capacitance contributions for nitrogen-doped reduced graphene oxide in acidic and alkaline electrolytes, 227 (2013) 300-308.

[4] J. Duay, S.A. Sherrill, Z. Gui, E. Gillette, and S.B. Lee, Self-limiting electrodeposition of hierarchical MnO_2 and $M(OH)_2/MnO_2$ nanofibril/nanowires: mechanism and supercapacitor properties, 7(2) (2013) 1200-1214.

[5] S.A. Ahmad, M.Z.U. Shah, M. Arif, M.S.U. Shah, E. Ullah, A. Shah, M. Sajjad, J. Aftab, and P. Song, Rational design of a novel MnO_2-$FeSe_2$ nanohybrid with nanowires/cubic architecture as promising supercapattery electrode materials, 936 (2023) 117318.

[6] N. Swain, S. Balasubramaniam, and A. Ramadoss, High energy density supercapattery empowered by efficient binder-free three-dimensional carbon coated $NiCo_2O_4$/Ni battery and Fe_3S_4@ NiCo pseudocapacitive electrodes, 58 (2023) 106220.

[7] M. Shaheen, M.Z. Iqbal, M.W. Khan, S. Siddique, S. Aftab, and S.M. Wabaidur, Fuels, Evaluation of a Redox-Active Cu-MOF and Co-MOF as Electrode Materials for Battery–Supercapacitor-Type Hybrid Energy Storage Devices, 37(5) (2023) 4000-4009.

[8] S. Raj, P. Kar, and P. Roy, Facile synthesis of flower-like morphology $Cu_{0.27}Co_{2.73}O_4$ for a high-performance supercapattery with extraordinary cycling stability, 54(87) (2018) 12400-12403.

[9] R. Manikandan, A.D. Savariraj, G. Nagaraju, A. Kale, J. Puigdollers, H. Park, H.S. Kim, J.M. Oh, C.J. Raj, and B.C. Kim, Mixed-phase composites derived from cobalt terephthalate as efficient battery-type electrodes for high-performance supercapattery, 157 (2023) 220-233.

[10] Q. Hu, M. Tang, M. He, N. Jiang, C. Xu, D. Lin, and Q. Zheng, Core-shell MnO_2@CoS nanosheets with oxygen vacancies for high-performance supercapattery, 446 (2020) 227335.

[11] S.K. Babu, and B. Gunasekaran, Ultrathin α-$Ni(OH)_2$ nanosheets coated on MOF-derived Fe_2O_3 nanorods as a potential electrode for solid-state hybrid supercapattery device, 447 (2023) 142146.

[12] W. Liu, J.L. Cheong, M.F. Ng, and J.Y. Ying, Carbon Nitride Mediated Synthesis of Titanium-Based Electrodes for High-Performance Asymmetric Supercapacitors, (2023) 108489.